# Terminal Electron Acceptors Influence the Quantity and Chemical Composition of Capsular Exopolymers Produced by Anaerobically Growing *Shewanella* spp.

Andrew L. Neal,*,† Steven N. Dublin,‡ Jeanette Taylor,‡ David J. Bates,§ Justin L. Burns,§ Robert Apkarian,‡ and Thomas J. DiChristina§

*Savannah River Ecology Laboratory, The University of Georgia, Aiken, South Carolina 29802, The Integrated Microscopy and Microanalytical Facility, Emory University, Atlanta, Georgia 30322, and School of Biology, Georgia Institute of Technology, Atlanta, Georgia 30332*

*Received August 25, 2006; Revised Manuscript Received October 16, 2006*

Bacterial exopolymers perform various roles, including acting as a carbon sink, a protective layer against desiccation or antimicrobial agents, or a structural matrix in biofilms. Despite such varied roles, little is known about the heterogeneity of bacterial exopolymer production under varying growth conditions. Here we describe experiments designed to characterize the quantity and quality of exopolymers produced by two commonly studied members of the widely distributed genus *Shewanella*. Electrokinetic, spectroscopic, and electron microscopic techniques were employed to demonstrate that cell surfaces of *Shewanella oneidensis* MR-1 (electrophoretic softness, $\lambda^{-1}$, range from 0.4 to 2.6 nm) are associated with less extracellular polymeric material than surfaces of *Shewanella putrefaciens* 200R ($\lambda^{-1}$ range from 1.6 to 3.0 nm). Both species exhibit similar responses to changes in electron acceptor with nitrate- and fumarate-grown cells producing relatively little exopolymer compared to trimethylamine *N*-oxide (TMAO)-grown cells. In *S. oneidensis*, the increase in exopolymers has no apparent effect upon cell-surface fixed charge density (−7.7 to −8.7 mM), but for *S. putrefaciens* a significant drop in fixed charge density is observed between fumarate/nitrate-grown cells (−43 mM) and TMAO-grown cells (−20.8 mM). For both species, exopolymers produced during growth on TMAO have significant amide functionality, increasing from approximately 20−25% of C-containing moieties in nitrate-grown cells to over 30% for TMAO-grown cells (determined from X-ray photoelectron spectroscopy). The increased exopolymer layer associated with TMAO-grown cells appears as a continuous, convoluted layer covering the entire cell surface when viewed by low-temperature, high-resolution scanning electron microscopy. Such significant changes in cell-surface architecture, dependent upon the electron acceptor used for growth, are likely to influence a variety of cell interactions, including aggregation and attachment to surfaces, and the binding of aqueous metal species.

## Introduction

The genus *Shewanella* is represented by a large number of facultative anaerobes isolated from diverse environments. *S. oneidensis* MR-1 was isolated from metal-rich lacustrine sediments;[1] other members have been isolated from rotting fish and clinical settings[2−4] (*S. putrefaciens*), as well as marine environments including biofilms (*S. baltica*,[5] *S. colwelliana*[6]) and in the proximity of hydrothermal vents[7] (*S. ioihica*). Given this wide distribution, *Shewanella* species are postulated to be important to the cycling of carbon as well as various metals. *Shewanella* are able to respire a wide range of electron acceptors whose redox potential almost spans the entire continuum.[8] Particular research interest in members of the genus is derived from the respiration of complexed and solid metals during anaerobic respiration, for example, Fe, Mn, and U. See recent review by DiChristina et al.[9]

*Shewanella* spp. also produce novel cell-surface polysaccharides including phenol-soluble shewanellose produced by *S. putrefaciens* A6.[10] A number of unusual amino sugars have been isolated from *S. japonica* KMM 3299[11] and a lipo-oligosaccharide containing 2,3-dihydroxypropanoic acid from *S. pacifica*.[12] Comparison of a number of commonly studied *Shewanella* species indicates that lipopolysaccharide type (rough or smooth) and the presence and degree of development of a capsule is species-dependent.[13] Capsule layers of 16 isolates ranged from 20−130 nm in thickness. The cell surface of *S. putrefaciens* CN-32 was found to be free of any capsular material. Lipopolysaccharides of *S. putrefaciens* and *S. oneidensis* do not have *O*-acetyl side chains (and are termed rough LPS accordingly) while those of *S. amazonensis* and *S. algae* are smooth, possessing side chains.

Production of surface exopolymers has been studied only under a limited range of growth conditions, typically in rich media. For example, polysaccharides from *S. japonica* KMM 3299, *S. algae* 48055, and *S. putrefaciens* strains A6 and S29 have all been studied in a Yoshimizu-Kimura medium,[10,11,14] while polysaccharides from *S. pacifica* have been isolated from cells growing in a medium containing glucose, peptone, and yeast extract.[12] Only polysaccharides produced by *S. oneidensis* MR-4 have been studied in contrasting media.[15] In this case, the different growth media resulted in switching of *N*-acylation of a 4-amino-4,6-dideoxy-D-glucose moiety from 3-hydroxybutyrate in minimal medium to 3-hydroxy-3-methylbutyrate in tryptic soy broth. The variability of exopolymer production in

* To whom correspondence should be addressed. Savannah River Ecology Laboratory, The University of Georgia, PO Drawer E, Aiken, SC 29802. E-mail: neal@srel.edu. Phone: (803)725 5341.

† The University of Georgia.

‡ Emory University.

§ Georgia Institute of Technology.

10.1021/bm060826e CCC: $37.00 
Published on Web 12/01/2006

*Shewanella* spp. remains poorly understood, especially with regard to growth on different terminal electron acceptors.

To test the hypothesis that the quantity and quality of cell-surface-associated exopolymers is dependent upon cell growth conditions, *S. oneidensis* and *S. putrefaciens* were grown separately on three anaerobic terminal electron acceptors. The inclusion of metalliferous electron acceptors (e.g., the ferric, manganic, chromate, or uranyl ions) presents many problems to the study of surface physicochemistry of bacterial cells. Principally, the formation of metal precipitates following reduction in association with the cell surface or associated exopolymers precludes the study of the cell outer membrane in isolation. For this reason, we chose non-metalliferous terminal electron acceptors, two of which (nitrate and fumarate) are typically associated with natural anaerobic sediments or waters and the other, trimethylamine *N*-oxide, typically associated with protein-rich tissues of marine animals (fish, squid, etc.). Whole cell microelectrophoresis, cell-surface spectroscopy, and electron microscopy techniques were employed to demonstrate that cells utilizing either fumarate or nitrate as a terminal electron acceptor display cell surfaces largely free of extracellular material. Cells respiring on trimethylamine *N*-oxide, however, produce significant quantities of extracellular material at the cell surface, which also contains a higher protein component than exopolymers produced during growth on nitrate or fumarate as a terminal electron acceptor.

## Materials and Methods

**Growth Media and Culture Conditions.** *Shewanella oneidensis* strain MR-1 and *S. putrefaciens* strain 200 cultures were grown at 25 °C. The growth medium consisted either of tryptic soy broth (TSB, Mo Bio Laboratories Inc.) at a concentration of 30 g $L^{-1}$ or a defined salt medium[16] (49 mM $(NH_4)SO_4$, 5.7 mM $K_2HPO_4{\cdot}3H_2O$, 3.3 mM $KH_2PO_4$, 2 mM $NaHCO_3$, 1 mM $MgSO_4{\cdot}7H_2O$, 500 $\mu$M $CaCl_2{\cdot}2H_2O$, 70 $\mu$M $Na_2EDTA{\cdot}2H_2O$, 60 $\mu$M $H_3BO_3$, 10 $\mu$M NaCl, 6 $\mu$M $FeSO_4{\cdot}7H_2O$, 5 $\mu$M $Ni(NH_4)(SO_4)_2{\cdot}6H_2O$, 4 $\mu$M $Na_2MoO_4{\cdot}2H_2O$, 1.5 $\mu$M $Na_2SeO_4$, 1.3 $\mu$M $MnSO_4{\cdot}H_2O$, 1 $\mu$M $ZnSO_4{\cdot}7H_2O$, and 0.2 $\mu$M $CuSO_4{\cdot}5H_2O$). The amino acids L-arginine, l-serine, and L-glutamic acid were added at a concentration of 0.02 mg $mL^{-1}$ and 30 mM lactate served as a both a carbon source and electron donor. For tryptic soy solid medium, Bacto agar (Difco) was added at 1.5% (w/v). Precultures were grown in TSB overnight at 25 °C on a shaking incubator (150 rpm). Cells were removed from the culture medium by centrifugation (2000*g*, 8 min, 4 °C) and washed three times in chilled, sterile 2 mM KCl (pH = 5.8). These washed cells were then used as inoculum for anaerobic cultures in a defined salt medium. Filter sterilized terminal electron acceptor stocks (fumarate, nitrate, or trimethylamine *N*-oxide) were added to a final concentration of 30 mM. Batch cultures (600 mL) were grown to a target optical density ($A_{470} = 1$). Cells were again washed three times as described above, this time in $O_2$-free 2 mM KCl. Washed cells were resuspended in 35 mL of sterile 2 mM KCl and stored on ice until use.

**Bacterial Cell Microelectrophoresis.** Bacterial cells possessing a layer of ion-penetrable polymers on their surface are poorly described by the classic Smoluchowsky equation typically used to determine surface parameters (zeta potential) of colloids and particles. For cells, more appropriate models (addressed below) have been developed which allow an estimation of the ion-penetrable layer thickness. These models require the measurement of cell electrophoretic mobility across a range of ionic strengths. Here, laser Doppler velocimetry was employed to estimate electrophoretic mobility at 25 °C (Zetasizer 3000$HS_A$, Malvern Instruments Ltd., Malvern, UK). Prior to each set of measurements, the mobility of a manufacturer-supplied polystyrene standard was measured to ensure accuracy of the measured cell mobilities. Measurements with cells were made over a wide range of KCl concentrations, from 5 to 300 mM (pH 5.5−5.8). Prior to measurement at each ionic strength, three conductance readings were carried out, polarizing the electrodes at each new concentration. Measurements of cell motility in the absence of an applied electrical field were also made and subtracted from the mobility estimates. Reported estimates and associated standard errors result from a total of 12 measurements, the sum of three measurements made on four independent, yet parallel, cell batches.

**Treatment of Cell Mobility Data.** According to Ohshima's approximate analytical expression for soft-particle electrokinetic behavior,[17] electrophoretic mobility ($\mu$) of soft particles is expressed as

$$\mu = \frac{\epsilon_0 \epsilon_r}{\eta} \frac{\psi_0/\kappa_m + \psi_{DON}/\lambda}{1/\kappa_m + 1/\lambda} + \frac{\rho_{fix}}{\eta \lambda^2}$$

where $\epsilon_0$ is the permittivity of vacuum, $\epsilon_r$ is the relative permittivity, and $\eta$ the viscosity of the medium. The exopolymer fixed charge density ($\rho_{fix}$) is defined by the number concentration ($N$) and valence ($Z$) of the dissociated functional groups in the exopolymer layer and by the elementary electric charge ($e$) according to

$$\rho_{fix} = NZe$$

The electrophoretic softness ($1/\lambda$) of the exopolymer layer is defined by

$$1/\lambda = \sqrt{\eta/\omega}$$

where $\omega$ is the friction coefficient for flow within the exopolymer. $1/\lambda$ is expressed in length units. The Donnan potential of the exopolymer layer ($\psi_{DON}$) is given by

$$\psi_{DON} = \frac{kT}{ze} \ln\left\{ \frac{\rho_{fix}}{2zen^\infty} + \sqrt{\left(\frac{\rho_{fix}}{2zen^\infty}\right)^2 + 1} \right\}$$

the outer surface potential ($\psi_0$) by

$$\psi_0 = \frac{kT}{ze}\left( \ln\left\{ \frac{\rho_{fix}}{2zen^\infty} + \sqrt{\left(\frac{\rho_{fix}}{2zen^\infty}\right)^2 + 1} \right\} + \frac{2zen^\infty}{\rho_{fix}}\left\{ 1 - \sqrt{\left(\frac{\rho_{fix}}{2zen^\infty}\right)^2 + 1} \right\} \right)$$

and the Debye-Hückel parameter of the exopolymer layer ($\kappa_m$) by

$$\kappa_m = \kappa\left[ 1 + \left(\frac{\rho_{fix}}{2zen^\infty}\right)^2 \right]^{1/4}$$

In the above expressions $k$ is the Boltzmann constant, $T$ is the absolute temperature, and $z$ and $n^\infty$ are the valence and bulk number concentration of the symmetrical electrolyte in solution, respectively. One drawback of the soft particle theory is its inability to predict the absolute thickness of the exopolymer since it does not probe beyond the thickness of the Debye-Hückel layer.[18] Electroosmotic flow occurs only through the outer layers of exopolymer at the cell surface. Soft particle theory, however, has successfully described the behavior of fibrillated and nonfibrillated *Streptococcus salivarius* strains.[19] In the present study, soft particle theory is employed in conjunction with electron microscopy, to compare the relative thickness of exopolymers produced on surfaces of *S. putrefaciens* and *S. oneidensis* cells grown anaerobically on fumarate, nitrate, and TMAO as terminal electron acceptors.

**Attenuated Total Reflection-Fourier Transform Infrared Spectroscopy.** ATR-FTIR probes the chemistry of samples interacting with an evanescent wave created at the surface of an internal reflection element. As such, the information collected derives predominantly, though not exclusively, from the surface of the sample. Spectra were collected from lawns of KCl-washed cells supported on 0.45 $\mu$m pore

cellulose triacetate filters (Millipore, Bedford, MA). Supported lawns were dried under a stream of $N_2$ until dry (typically 30−60 min) to minimize the contribution of water to the collected spectra. ATR-FTIR was performed on a Magna 860 Fourier-transform infrared spectrometer (Nicolet, Thermo Corporation) equipped with a KBr beam splitter, wide band, liquid-$N_2$-cooled mercury−cadmium−telluride detector and a MVP2 Star attenuated total reflection accessory (Harrick Scientific Products, Inc., Pleasantville, NY) with a single-reflection diamond crystal internal reflection element. Typically, 2000 spectra were collected and averaged at a resolution of 2 $cm^{-1}$. A background spectrum collected in air was subtracted from spectra collected of the cell surfaces.

**X-ray Photoelectron Spectroscopy.** XPS is a near-surface sensitive technique providing information on elemental abundance and relative proportions of functional groups at the sample surface. Spectra were collected from lyophilized cell pellets. After washing in 2 mM KCl, cells were centrifuged at 2000*g* (20 min, 4 °C) and the supernatant was discarded. The resulting cell pellet was centrifuged a second time (10000*g*, 20 min, 4 °C) and immediately plunged into liquid $N_2$ until completely frozen. Once frozen, the cell pellet was introduced onto a Freezone 12 freeze-drying system (Labconco). Lyophilized cell pellets were mounted onto double-sided carbon tape affixed to an XPS sample holder. Cells were pressed onto the tape surface using a PTFE block. Once mounted, the cells were introduced into the spectrometer. Spectra were collected on a Physical Electronics 5600ci spectrometer (Perkin-Elmer, Eden Prairie, MN). The spectrometer was calibrated employing the Au $4f_{7/2}$, Cu $2p_{3/2}$, and Ag $3d_{5/2}$ photopeaks with binding energies ($E_B$) of 83.99, 932.66, and 368.27 eV, respectively. A consistent 400 $\mu$m spot size was analyzed on all cell surfaces using a monochromatised Al K$\alpha$ X-ray source ($h\nu$ = 1.487 keV) at 300 W and a pass energy of 46.95 eV for low-resolution scans, and 11.75 eV for high-resolution scans. The system was operated at a base pressure between $10^{-8}$ and $10^{-9}$ Torr. A 5 eV electron flood gun was used to compensate for sample charging; additionally, the $C-H_{aliphatic}$ C 1s photopeak was set at a consistent $E_B$ of 284.8 eV.

**Electron Microscopy.** Bacterial culture pellets were washed in 100 mM sodium cacodylate buffer (pH 7.4) for 15 min and fixed with 2.5% TEM-grade glutaraldehyde in sodium cacodylate buffer for 18−24 h. Following fixation, samples were again washed in 100 mM sodium cacodylate buffer three times for 10 min each. Additional $dH_2O$ washes were performed twice for 10 min each prior to fixation in 1% $OsO_4$ for 1 h. After two $dH_2O$ washes, the sample was dehydrated through a graded ethanol series in steps of 10 min each: 30%, 50%, 70%, 80%, and 90%, ending in two changes of 100% dry ethanol. Dehydration was completed with two changes of propylene oxide (PPO) of 10 min each. Next, the sample was infiltrated with EMbed 812 (Electron Microscopy Sciences, Hatfield, PA) epoxy resin in three stages: 1:1 mixture of PPO and resin for 2 h to overnight with gentle mixing, 1:2 mixture of PPO and resin for 2 h to overnight with gentle mixing, and two changes of 100% epoxy resin for 2 h to overnight under vacuum. Cells were embedded in fresh epoxy resin in labeled conical Beem capsules and evacuated for 2 h. The embedded cells were polymerized for 4 days at 60 °C. Selected blocks were trimmed and thick (0.5−1.0 $\mu$m) sections were collected on glass slides and stained with 1% (aq) Toluidine Blue O. Selected blocks were trimmed and thin-sectioned (70−80 nm) using a diamond knife and an RMC MT-7000 ultramicrotome. Thin sections were collected on 200 mesh copper grids and post-stained for 10 min each with 5% uranyl acetate and Reynold's lead citrate and subsequently imaged using a JEOL JEM-1210 transmission electron microscope (TEM) at 90 kV.

For low-temperature sample preparation, 2.5 $\mu$L of a concentrated cell pellet was gently pipetted onto 3 mm gold planchets (Balzers, 012 0130T) and briefly inverted to collect the pellet mass on the droplet surface. The sample was then plunge-frozen in liquid ethane (−183.3 °C) and stored under liquid $N_2$. Next, the sample was transferred to a precooled (−170 °C) Oxford CT-3500 cryostage, where the specimen surface was fractured with a prechilled blade and washed with liquid $N_2$. Immediately following fracture, the stage shutters were closed and the cryostage transferred to a Denton DV-602 chromium coater, where the sample was held under a constant vacuum of $4 \times 10^{-7}$ Torr. Cryoetching was performed in the chromium coater by gradually increasing the sample temperature from −180 to −105 °C using an Oxford ITC 502 temperature controller and maintaining the sample temperature at −105 °C for 15−17 min. The etched sample was then sputter-coated with 2 nm of chromium and rapidly transferred to the upper stage of a Topcon DS-130 field emission scanning electron microscope. Low-temperature−high-resolution scanning electron microscopy (LT−HRSEM) images were collected from whole-cell samples. Imaging was performed at 25 kV following 30 min of temperature stabilization at −120 °C.

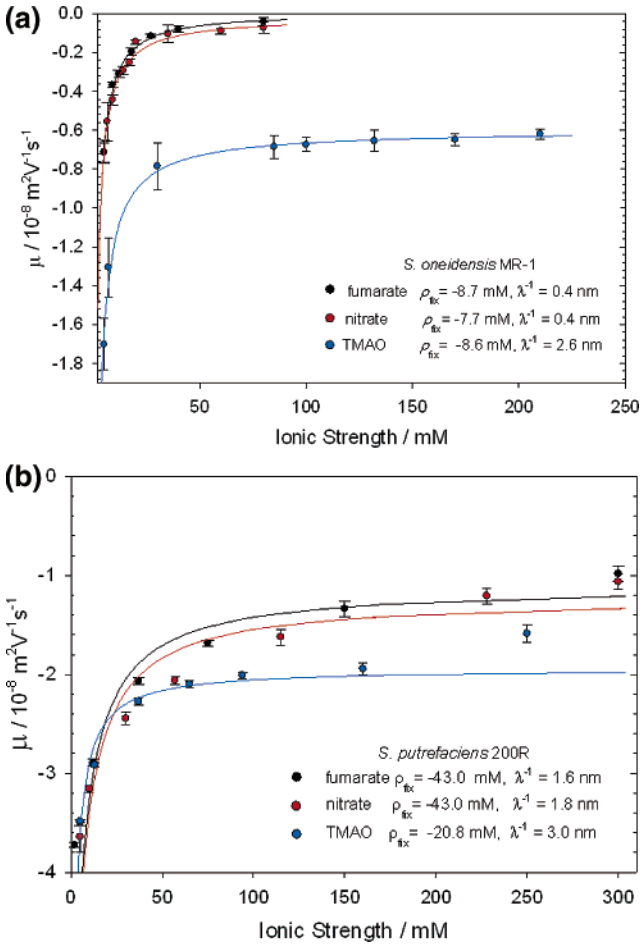


**Figure 1.** Electrophoretic mobility ($\mu$) estimates in KCl solutions (pH 5.8) as a function of ionic strength for *S. oneidensis* and *S. putrefaciens* grown with different electron acceptors. The solid lines represent the best fit to Ohshima's soft particle model. Error bars indicate the standard error of 12 measurements made with four batches of cells.

## Results

***S. oneidensis* Cell Electrophoretic Mobility.** Cells grown on fumarate, nitrate, and TMAO displayed distinctly different electrophoretic mobility ($\mu$) with increasing solution ionic strength (Figure 1). Cells grown on all terminal electron acceptors exhibited negative electrophoretic mobilites, indicating that, under each growth condition, *S. oneidensis* MR-1 cells display a net negative surface charge. However, for fumarate- and nitrate-grown cells, $\mu$ dropped rapidly between 5 and 26 mM for both fumarate- and nitrate-grown cells. Above this concentration, $\mu$ more gradually approached zero at 80 mM.

**Table 1.** Estimates (±95% Confidence Intervals) of Fixed Charge Potential ($\rho_{fix}$) and Electrophoretic Softness ($\lambda^{-1}$) for Cells of *S. oneidensis* MR-1 and *S. putrefaciens* 200 Grown on Different Electron Acceptors[a]

| | *S. oneidensis* MR-1 | | | *S. putrefaciens* 200 | | |
|---|---|---|---|---|---|---|
| | fumarate | nitrate | TMAO | fumarate | nitrate | TMAO |
| $\rho_{fix}$/mM | $-8.7 \pm 1.7$ | $-7.7 \pm 1.2$ | $-8.6 \pm 1.5$ | $-43.0 \pm 38.8$ | $-43.0 \pm 32.7$ | $-20.8 \pm 0.9$ |
| $\lambda^{-1}$/nm | $0.4 \pm 0.6$ | $0.4 \pm 0.6$ | $2.6 \pm 0.4$ | $1.6 \pm 0.9$ | $1.8 \pm 0.9$ | $3.0 \pm 0.7$ |
| $r^2$ | 0.996 | 0.991 | 0.992 | 0.941 | 0.894 | 0.999 |

[a] The estimates are derived from fitting electrophoretic mobility data to Ohshima's approximate analytical expression for soft-particle electrokinetic behavior (see Materials and Methods section for details). The coefficients of determination ($r^2$) for each data set are also shown.

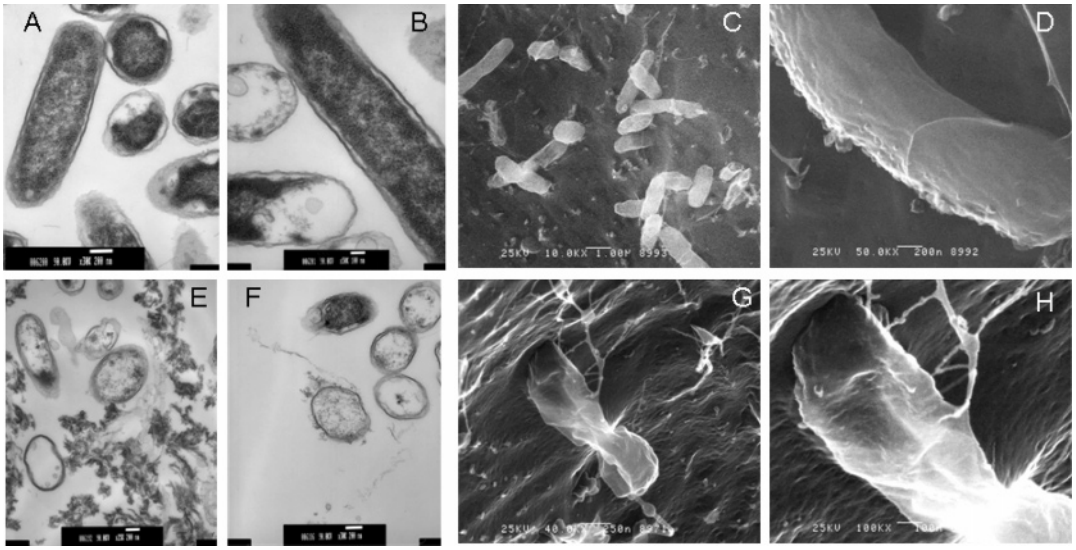


**Figure 2.** Electron micrographs of 5% uranyl acetate and Reynold's lead citrate stained *S. oneidensis* grown either with fumarate (A, B) or TMAO (E, F) as sole electron acceptor. Corresponding LT−HRSEM micrographs of chromium-coated cells grown with fumarate (C, D) or TMAO (G, H) are also shown. Accumulation of exopolymers on the outer cell surface of TMAO-grown cells is clearly evident.

Due to the difficulty in collecting reliable mobility estimates so close to zero, electrophoretic measurements were not performed above this ionic strength for either fumarate- or nitrate-grown cells. In contrast, TMAO-grown cells displayed a significantly nonzero $\mu$ of approximately $-0.7 \times 10^{-8}$ m$^2$ V$^{-1}$ s$^{-1}$ at ionic strengths in the 75−220 mM range.

***S. putrefaciens* Cell Electrophoretic Mobility.** In contrast to *S. oneidensis*, *S. putrefaciens* maintained significantly nonzero electrophoretic mobility above 80 mM, regardless of the terminal electron acceptor utilized. For fumarate-grown cells a mobility of $-1.3 \pm 0.080 \times 10^{-8}$ m$^2$ V$^{-1}$ s$^{-1}$ was observed at 150 mM KCl; for nitrate-grown cells $\mu = -1.6 \pm 0.078 \times 10^{-8}$ m$^2$ V$^{-1}$ s$^{-1}$ at 115 mM; and for TMAO-grown cells $\mu = -1.9 \pm 0.060 \times 10^{-8}$ m$^2$ V$^{-1}$ s$^{-1}$ at 160 mM.

**Estimates of Fixed Charge Potential and Electrophoretic Softness.** Results of fitting the electrophoretic mobility data collected for *S. oneidensis* MR-1 cells grown with fumarate, nitrate, or TMAO as a terminal electron acceptor to Ohshima's equation are given in Table 1; the fitted models are shown in Figure 1. All data sets agree well with the theoretical mobility estimates ($r^2$ of 0.996, 0.991, and 0.992 for the fumarate-, nitrate-, or TMAO-grown cells, respectively). Curve fitting indicates that nitrate-grown cells have a fixed charge density of $-7.7 \pm 1.2$ mM (estimate ±95% confidence interval of the estimate) and an apparent electrophoretic softness of $0.4 \pm 0.6$ nm. For fumarate-grown cells the estimates are not significantly different from the nitrate-grown estimates ($\rho_{fix} = -8.7 \pm 1.7$ mM; $\lambda^{-1} = 0.4 \pm 0.6$ nm). In agreement with the observation that $\mu$ approaches 0 m$^2$ V$^{-1}$ s$^{-1}$ at an ionic strength of approximately 80 mM, the electrophoretic softness estimate for both sets of cells is not significantly different from zero. In contrast, the fitted estimates for the TMAO-grown cells are $\rho_{fix} = -8.6 \pm 1.5$ mM and $\lambda^{-1} = 2.6 \pm 0.4$ nm, suggesting that while the fixed charge potential for the cells grown on the three terminal electron acceptors are not significantly different from each other, electrophoretic softness estimates are. This finding indicates that MR-1 cells respiring on TMAO as the electron acceptor produce a more extensive layer of extracellular material than cells respiring on either fumarate or nitrate, yet the overall net charge at the cell surface remains unchanged.

Although the mobility data for *S. putrefaciens* generally fit the model less well than *S. oneidensis* ($r^2$ of 0.941, 0.894 and 0.999 for the fumarate-, nitrate- or TMAO-grown cells, respectively), a similar trend in mobility (and consequently $\rho_{fix}$ and $\lambda^{-1}$) is observed for the three electron acceptors. For *S. putrefaciens*, fumarate-grown cells have a fixed charge potential of $-43.0 \pm 38.8$ mM and an electrophoretic softness of $1.6 \pm 0.9$ nm. These estimates are similar to those for nitrate-grown cells ($\rho_{fix} = -43.0 \pm 32.7$ mM and $\lambda^{-1} = 1.8 \pm 0.9$ nm). Unlike *S. oneidensis*, however, cells grown on TMAO as the electron acceptor display a reduced fixed charge potential of $-20.8 \pm 0.9$ mM: the increased electrophoretic softness ($\lambda^{-1} = 3.0 \pm 0.7$ nm). The observed trend is similar to that observed for *S. oneidensis* cells in this set of electron acceptors.

**Electron Microscopy.** To provide visual support for the electrophoretic softness predictions from cell mobility measurements, conventional transmission electron microscopy (TEM) of fixed, dehydrated cells and LT−HRSEM of unfixed, hydrated cells were employed to examine cell-surface features. Figure 2 shows images of *S. oneidensis* cells grown with either fumarate (Figures 2A−2D) or TMAO (Figures 2E−2H) as the terminal electron acceptor. In agreement with electrokinetic measurements, fumarate-grown cells displayed little, if any, polymers at the outer membrane surface. In contrast, TEM of TMAO-

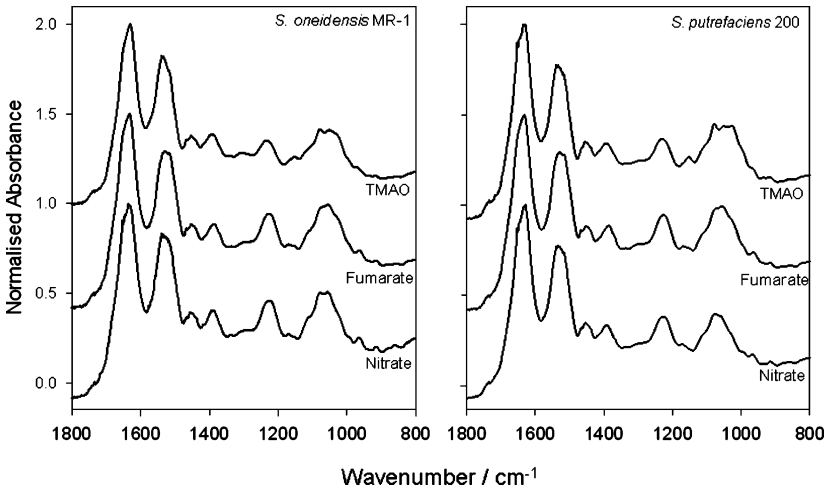


**Figure 3.** ATR-FTIR spectra of the outer cell surface of *S. oneidensis* and *S. putrefaciens* grown with different terminal electron acceptors.

grown cells indicates areas rich in amorphous background material only loosely associated with cell surfaces (Figure 2E). Other cells have significant accumulation of exopolymers at the cell surface (Figure 2F). Polymers streaming away from the cell surface are observed. Thus, observations of the cell surface using conventional TEM concur with electrophoretic softness estimates, suggesting that fumarate-grown cells produce little, if any, exopolymer while TMAO-grown cells produce significant exopolymeric material. Due to the fixation and dehydration steps necessary for TEM, however, an appreciation cannot be gained of the architecture of the outer-membrane surface (also a drawback of conventional SEM). LT−HRSEM, which requires neither fixation nor dehydration of cells, permits visualization of cells in a fully dehydrated state. In agreement with the previously described TEM images, LT−HRSEM indicates that the surface of fumarate-grown MR-1 cells are free of exopolymers (Figure 2C), a finding confirmed by high magnification of the cell surface (Figure 2D). The ability of LT−HRSEM to visualize cell-surface architecture is best demonstrated with images collected from TMAO-grown cells. The accumulated exopolymer layers appear as a furrowed envelope obscuring the outer-membrane surface (Figure 2G). Other surface features include a polar flagellum and highly branched polymers streaming away from the cell surface. At higher magnification (Figure 2H) a number of surface features are observed emerging from the exopolymer layer (ranging in size between 10 and 20 nm in width). Thus, LT−HRSEM reveals that the surface of TMAO-grown cells is more complex in architecture than that of fumarate-grown cells: the exopolymer layer surrounding the cell also includes features that form highly branched structures of at least a cell length. A similar relationship was observed for *S. putrefaciens* cells (not shown).

**Infrared Spectroscopy.** Representative ATR-FTIR spectra collected from the surface of cells supported on cellulose acetate filters are shown in Figure 3. Peaks observed from cell surfaces are typical of spectra collected from Gram negative bacteria with peaks characteristic of the amide I and amide II vibrations of proteins with absorption maxima at approximately 1650 and 1530 $cm^{-1}$, respectively. The amide I band is confounded with water absorption at 1630 $cm^{-1}$. A broad complex absorption feature centered at 1100 $cm^{-1}$ derives from $\nu$C−C, $\nu$C−OH, and $\nu$C−O−C of carbohydrates as well as $\nu_s$P═O of phosphate groups associated with phospholipids and possibly phosphorylated carbohydrates. A strong absorption is observed for $\nu_{as}$P═O at approximately 1230 $cm^{-1}$.[20] Absorptions of lower intensity are observed at approximately 1456 $cm^{-1}$ due to $\delta CH_2$ and at

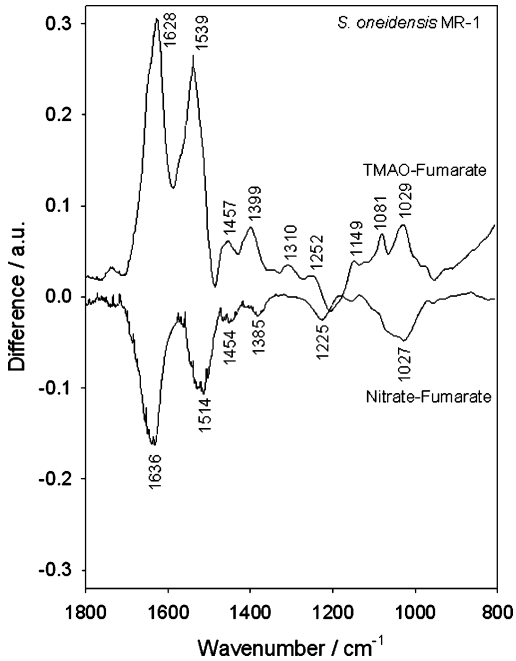


**Figure 4.** (Fumarate−nitrate) and (fumarate−TMAO) ATR-FTIR difference spectra of *S. oneidensis* cells. Approximate band positions are indicated in the figure.

1385 $cm^{-1}$ due to $\nu_s COO^-$. Other absorptions are due to terminal C−$CH_3$ rocking at approximately 964 $cm^{-1}$, asymmetric carbohydrate ring vibrations at approximately 916 $cm^{-1}$, and $\nu_{as}$C−O of axial OAc groups at approximately 1170 $cm^{-1}$.[21] Calculation of difference spectra highlights the difference in exopolymer content between fumarate-, nitrate-, and TMAO-grown cells.

Difference spectra resulting from nitrate−fumarate and TMAO−fumarate subtractions for *S. oneidensis* MR-1 are displayed in Figure 4. The primary difference between the two spectra is the sign of the difference spectra themselves. The nitrate−fumarate difference spectrum is largely negative, suggesting that exopolymers were more abundant on the fumarate-grown than nitrate-grown cells. The largest difference corresponds to the amount of proteinaceous moieties (significant negative peaks associated with amide I and II vibrations). Smaller differences in the amount of general carbohydrate (complex absorption feature at approximately 1027 $cm^{-1}$) and phosphate groups ($\nu_{as}$P═O at 1225 $cm^{-1}$) are also observed. In contrast, the TMAO−fumarate difference spectrum is positive

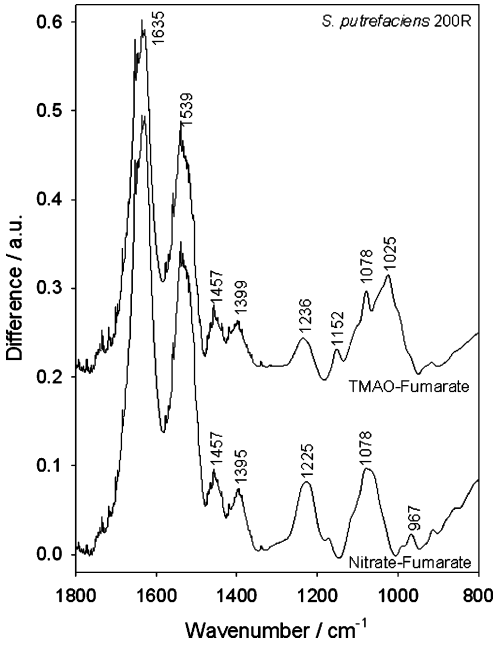


**Figure 5.** (Fumarate−nitrate) and (fumarate−TMAO) ATR-FTIR difference spectra of *S. putrefaciens* cells. Approximate band positions are indicated in the figure.

and the differences are greater in magnitude than those observed for the nitrate−fumarate difference spectrum. This finding suggests that the surface of TMAO-grown cells accumulates a greater amount of exopolymer than fumarate-grown cells. The primary difference again corresponds to the amount of protein associated with the cell surface and also reflects a general increase in absorption due to carbohydrates (complex absorption feature at 1029 and 1081 $cm^{-1}$). Peaks are also observed at 1149 $cm^{-1}$ corresponding to $\nu_{as}C-O$ of *O*-acetyl groups and at 1399 $cm^{-1}$ corresponding to $\nu_{as}COO^-$. In terms of chemistry, the surface of TMAO-grown cells is more complex, deriving from an increase in general protein and carbohydrate moieties as well as the presence of *O*-acetyl groups, not present on either fumarate- or nitrate-grown cell surfaces.

The difference spectra resulting from nitrate−fumarate and TMAO−fumarate subtractions for *S. putrefaciens* 200 are given in Figure 5. Both difference spectra are positive, indicating that both the nitrate-grown and the TMAO-grown cells accumulate more exopolymers at the cell surface than the fumarate-grown cells. Increases in both proteins and carbohydrates are apparent for both difference spectra as well as for $\nu_sCOO^-$ at 1395 and 1399 $cm^{-1}$ and $\nu_{as}P{=}O$ at 1225 and 1236 $cm^{-1}$ for nitrate- and TMAO-grown cells, respectively. Unique to the TMAO−fumarate difference spectrum (and in common with the TMAO−fumarate difference spectrum for *S. oneidensis*) is an increase in $\nu_{as}C-O$ of *O*-acetyl groups at 1152 $cm^{-1}$ and the presence of a peak at 1078 $cm^{-1}$ consistent with that observed for *S. oneidensis* at 1081 $cm^{-1}$. Assignment of this peak is difficult due to the various vibrations which give rise to absorption in this region. The position would be consistent with $\nu_sC-O$ of *O*-acetyl groups.

ATR-FTIR therefore indicates that the chemical composition of the exopolymer layer in both *S. oneidensis* and *S. putrefaciens* depends upon the electron acceptor used for growth. One clear difference between the two species is the increase in phosphate groups at the *S. putrefaciens* cell surface after growth on either nitrate or TMAO, a finding not observed on the *S. oneidensis* cell surface. Common to both species is an increase in *O*-acetyl groups, specifically during respiration on TMAO.

**X-ray Photoelectron Spectroscopy.** XPS presents two complementary approaches for interrogating the chemistry of the outer cell surface. The first approach is to compare the O/C and N/C ratios determined from the O 1s, N 1s, and C 1s core photopeak intensities (taking into account instrument sensitivity factors). When these ratios are compared to the electrophoretic softness ($\lambda^{-1}$) of *S. oneidensis* cells grown with the three electron acceptors (Figure 6a), qualitative differences in the chemistry of the outer membrane are detected. For *S. oneidensis*, both O/C and N/C increase with $\lambda^{-1}$, confirming an increase in $\lambda^{-1}$ is associated with a general increase in carbohydrate and protein moieties. In the case of fumarate- and nitrate-grown cells, O/C and N/C ratios are relatively similar, supporting the electrophoretic data. TMAO-grown *S. oneidensis* cells however, display increased O/C and N/C ratios, an indication that both carbohydrate and protein moieties are present. For *S. putrefaciens* (Figure 6b), the relationship between $\lambda^{-1}$ and elemental ratios differs: a negative relationship is observed between $\lambda^{-1}$ and O/C. Consistent with the trend observed for *S. oneidensis*, the nitrate- and fumarate-grown cells behave in a relatively similar manner, while TMAO-grown cells are again different. The N/C ratio for *S. putrefaciens* is consistent with that observed for *S. oneidensis* with a positive relationship between $\lambda^{-1}$ and N/C, while TMAO-grown cells again exhibit both an increased $\lambda^{-1}$ and N/C ratio. These results indicate that, in TMAO-grown cells, an increased $\lambda^{-1}$ results from the production of a predominantly proteinaceous exopolymer layer at the expense of carbohydrate moieties found associated with the relatively soft nitrate- and fumarate-grown cell surfaces. This finding is in contrast to that observed in the hard *S. oneidensis*, where an increase in $\lambda^{-1}$ of nitrate- or fumarate-grown cells compared to TMAO-grown cells is associated with a general increase in both carbohydrate and protein.

The second approach is to determine the relative contribution of functional groups determined by curve fitting to the convoluted C 1s photopeak at approximately 285 eV.[22] Results of curve fitting are shown in Table 2. In both strains, a reduction in *C*−H,C contributions (hydrocarbons) at 284.8 eV is apparent for nitrate-grown than for TMAO-grown cells. Concomitantly, an increase in *C*−O,N (alcohols, ethers, amides, or amines) contributions is observed. This data suggests that both strains produce greater quantities of amino moieties with TMAO as the electron acceptor than with nitrate. A trend in *C*═O (carbonyls, carboxylates, and amides) spectral contributions is less clear. While the contribution of *C*═O groups is higher in TMAO-grown cells than in nitrate-grown cells of *S. oneidensis*, the greatest *C*═O contribution at the *S. putrefaciens* cell surface is found in fumarate-grown cells.

## Discussion

The terminal electron acceptor used for anaerobic growth has a significant influence upon the amount and chemistry of exopolymers produced by *S. oneidensis* and *S. putrefaciens*. For both species, cells grown on nitrate or fumarate display outer membrane surfaces relatively free of exopolymers compared to TMAO-grown cells (Figures 1 and 2). In addition, exopolymers of both strains grown with TMAO contain the highest protein content (Table 2). *S. putrefaciens* produces the thicker capsule of the two species under all growth conditions. This finding is exemplified by the electrophoretic softness estimates, which for *S. oneidensis* increases from 0.4 nm for fumarate-grown to 2.6 nm for TMAO-grown cells. In contrast, the estimates increase from 1.6 to 3.0 nm for *S. putrefaciens*. Thus,

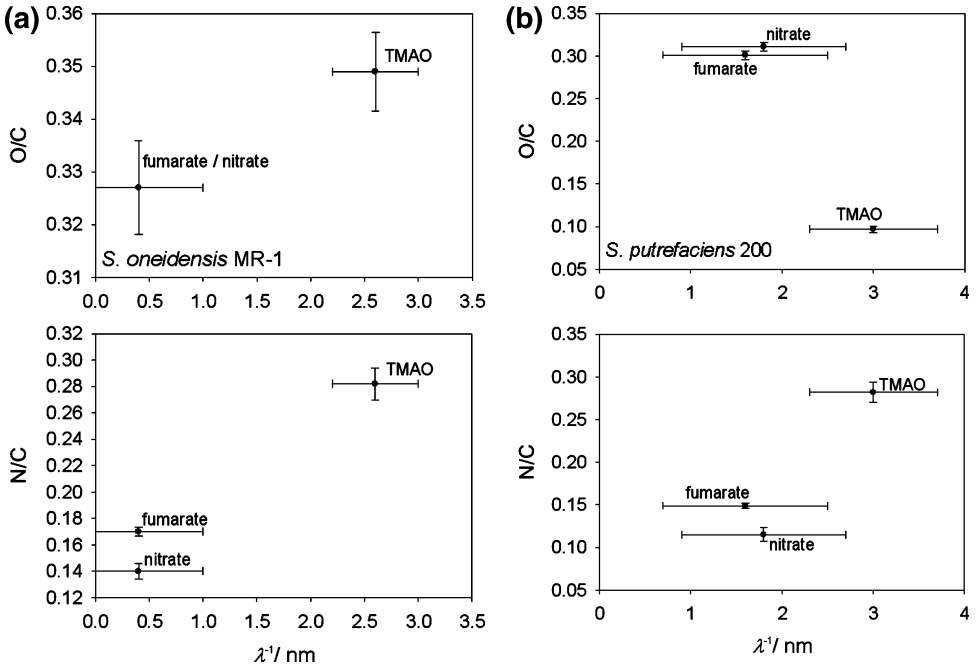


**Figure 6.** O/C and N/C elemental ratios determined from XPS of (a) *S. oneidensis* and (b) *S. putrefaciens* cell surfaces under the three terminal electron acceptor conditions, as a function of cell electrophoretic softness ($\lambda^{-1}$) from Table 1.

**Table 2.** Percentage of Different C-Containing Functional Groups Present on the Outer Cell Surface of *S. oneidensis* MR-1 and *S. putrefaciens* 200 as Determined by Curve-fitting in the C 1s Core Photopeak Region of XPS Spectra Collected from Lyophilized Cell Pellets[a]

| | | *C*−H,C 284.8 eV | *C*−O,N 286.2 eV | *C*═O 288.0 eV |
|---|---|---|---|---|
| MR-1 | nitrate | 64.9 | 20.5 | 14.7 |
| | fumarate | 53.7 | 29.6 | 16.7 |
| | TMAO | 46.0 | 35.8 | 18.2 |
| 200 | nitrate | 64.0 | 24.5 | 11.5 |
| | fumarate | 58.3 | 26.4 | 15.3 |
| | TMAO | 54.0 | 32.3 | 13.7 |

[a] Figures represent the means of the average of three estimates with a standard error of approximately 2%.

the difference between the two species is most pronounced for cells grown on either nitrate or fumarate. Increased exopolymer production by TMAO-grown cells renders this difference negligible. Despite increases in the amount of exopolymer produced at the cell surface, fixed charge potential ($\rho_{fix}$) for MR-1 does not differ significantly between the three terminal electron acceptors. As a consequence, extracellular processes dominated by electrostatic interactions, such as adsorption of metal ions and long-range cell−solid surface interactions, are likely to be unaffected by the presence of an increased capsule layer because the absolute concentration of charged functional groups remains unchanged. Only in TMAO-grown *S. putrefaciens* cells does the increase in surface-associated exopolymer result in a significant drop in $\rho_{fix}$. This reduction in fixed charge potential on the cell outer surface will likely result in reduced adsorption of metal ions and weaker electrostatic interactions during adhesion. The estimates of $\rho_{fix}$ for *S. oneidensis* MR-1 and *S. putrefaciens* 200 reported here are in good agreement with those reported previously for *S. oneidensis* MR-4 and *S. putrefaciens* CN-32:[23] $\rho_{fix}$ of −8.7 mM for fumarate-grown *S. oneidensis* MR-1 compared to −10 mM for trypticase soy broth-grown *S. oneidensis* MR-4, and a $\rho_{fix}$ of −43.0 mM for fumarate-grown *S. putrefaciens* 200 compared to −40 mM for tryptic soy broth-grown *S. putrefaciens* CN-32.

The observation that *S. oneidensis* MR-1 displays a relatively electrophoretically hard cell surface is in agreement with previous studies of capsule production by MR-1. Following growth in tryptic soy broth, MR-1 produces a truncated, sparse capsule with a thickness of 10−20 nm,[13] compared to *S. algae* BrY which produces a capsule of 60−90 nm and *S. oneidensis* MR-4 with a capsule of 70−130 nm. In contrast to our observation that *S. putrefaciens* 200 produces a relatively thick capsule (even under nitrate or fumarate growth conditions), *S. putrefaciens* CN-32 and *S. putrefaciens* NCTC 10695 produce no capsule.[13] Electrophoretic softness estimates for fumarate-grown *S. putrefaciens* 200 cells (1.6 ± 0.9 nm) are in agreement with estimates from tryptic soy broth-grown *S. putrefaciens* CN-32 of 2 nm.[23] The aforementioned discrepancy may be due to differences in growth media, although the richer growth medium used for CN-32 and NCTC 10695 is expected to induce a thicker capsule. A second empirical difference between *S. oneidensis* and *S. putrefaciens* is the ability of Ohshima's theory to successfully explain cell electrophoretic mobility. The mobility data for *S. oneidensis* fit well with that predicted by the soft particle theory; however, the data for *S. putrefaciens* fit less well. One explanation for this difference is that soft particle theory assumes charge to be homogeneously distributed throughout the soft layer. Homogeneous charge distribution appears to be the case for *S. oneidensis* since theory is in agreement with experimental data. Lack of agreement between theory and the *S. putrefaciens* experimental data suggests a heterogeneous distribution of charge within the thicker exopolymer layer. Such heterogeneous charge distribution may reflect the presence of either neutral or negatively charged *O*-acetyl groups[13] associated with the lipopolysaccharide or capsule layer or the presence of an unidentified outer membrane protein.

Predictions from soft particle theory agree with observations of exopolymers associated with the outer membrane surfaces observed by both conventional TEM and LT−HRSEM (Figure 2). The increased exopolymer layer of TMAO-grown cells

appears as a continuous layer covering the complete cell surface. Other electron-translucent structures with widths between 10 and 20 nm are also evident, streaming away from the cell surface, but originating within the exopolymer layer. Although such structures are evident in fixed, dehydrated, and low-temperature-preserved cells, the actual architecture of the cell surface is only detected in low-temperature-preserved cells which remain in a hydrated state. A detailed chemical analysis of the exopolymers produced by the two species has yet to be performed. However, the spectroscopic techniques allow qualitative comparisons. Both ATR-FTIR and XPS indicate that TMAO-grown *S. oneidensis* and *S. putrefaciens* cells produce exopolymers with an increased protein component relative to either nitrate- or fumarate-grown cells. Differences in *O*-acetyl and deprotonated carboxyl groups are also apparent. *O*-Acetyl groups accumulate at the cell surface in direct response to TMAO respiration; peaks consistent with this functional group, $\nu_{as}C-O$ (and possibly $\nu_{s}C-O$), are only observed in spectra collected from the surface of TMAO-grown cells (Figure 4).

Extracellular polymers secreted by bacteria are typically composed of polysaccharides, proteins, and to a lesser degree nucleic acids and lipids. Such polymers are generally divided into capsules either tightly associated with the cell membrane or as free exopolymers that more readily dissociate from the cell surface and are highly soluble.[24] In the present study, we have observed capsular exopolymer production in *Shewanella* grown anaerobically on non-metalliferous electron acceptors. Although TMAO is associated with the accumulation of thicker capsular layers, the TMAO/trimethylamine midpoint potential ($E_0' = +130$ mV) lies between those of fumarate/succinate ($E_0' = +33$ mV) and $NO_3^-/NO_2^-$ ($E_0' = +430$ mV).[25] Thus, the amount of energy theoretically available from reduction does not appear to strongly influence the production of capsular material. This raises the possibility that increased production of capsular polymers, specifically containing increased amino functionality, results from assimilation of either TMAO or the reduced trimethylamine, with excess amino groups secreted from the cell. Alternatively, the lack of significant capsule development during respiration on those electron acceptors typically found in subsurface environments (nitrate and fumarate) may reflect the importance of cell−mineral contact during Fe(III) respiration. This would suggest that the cell surface of nitrate- and fumarate-grown cells is maintained in a capsule-free state in readiness for a switch to iron reduction once it becomes energetically efficient.

Differences in capsular exopolymer production and chemistry may significantly affect cell behavior in a variety of ways. Cell capsules are often implicated in adhesion. Classical DLVO theory has been used to successfully predict the sign of interaction forces between MR-1 cells and the iron oxides hematite and magnetite[26] (chosen because of their differing $pH_{PZC}$). As might be expected for cells lacking *O*-antigen,[13] long-range (10−100 nm) repulsive forces are not observed for either mineral surface. However, electrostatic repulsion is predicted by DLVO theory and observed for cells approaching a magnetite surface; a primary maximum is observed at approximately 2 nm separation. This demonstrates that, at least for adhesion to iron minerals, electrostatic interactions are important, and changes in cell-surface charge may be significant. The influence of terminal electron acceptor upon fixed charge potential appears to decrease only in TMAO-grown *S. putrefaciens* cells. The increase in capsular exopolymers produced by both species, however, may influence adhesion via alternative mechanisms. For example, the production of an extensive capsule in *Escherichia coli* MG1655 effectively masks the function of short adhesins including antigen 43 (Ag43), a self-recognizing adhesin responsible for cell aggregation and AIDA-I, a second surface-expressed adhesin.[27] An agglutination protein (AggA) is involved in auto-aggregation and biofilm formation by *S. oneidensis* MR-1.[28] Such outer membrane proteins may be influenced by the production of an extensive capsule in a similar manner to Ag43. Metal ion binding by bacterial exopolymers is a well-studied phenomenon[29,30] and arises from the net negative charge conferred to exopolymers by carboxyl, amine, phosphate, and sulfate functional groups.[31] The complexation of metals may confer a certain degree of structure to the exopolymer matrix. Metal binding by exopolymers may have detrimental effects, including hyperaccumulation of toxic metals such as tin,[32] or be beneficial when employed to remove metals from aqueous waste.[33] Current work is focused on relating the observed changes in exopolymer production to cell autoaggregation and metal binding capacity when grown on nitrate, fumarate, and TMAO as anaerobic electron acceptors.

**Acknowledgment.** The authors would like to thank Alexis de Kerchove (Department of Chemical Engineering, Yale University) for helpful discussion concerning the calculation of Ohshima's equations and three anonymous reviewers whose comments helped improve the manuscript. X-ray photoelectron spectroscopy was performed at The Image and Chemical Analysis Laboratory, Department of Physics, Montana State University, Bozeman, MT. This research was supported by the Office of Science (BER), U.S. Department of Energy, Grant DE-FG02-05ER64121.

## References and Notes

(1) Myers, C. R.; Nealson, K. H. *Science* **1988**, *240*, 1319−1321.
(2) Jorgensen, B. R.; Hu$\beta$, H. H. *Int. J. Food Microbiol.* **1989**, *9*, 51−62.
(3) Stenstrom, I.-M.; Molin, G. *J. Appl. Bacteriol.* **1990**, *68*, 601−618.
(4) Brink, A. J.; van Straten, A.; van Rensberg, A. J. *Clin. Infect. Dis.* **1995**, *20*, 1327−1332.
(5) Ziemke, F.; Hofle, M. G.; Lalucat, J.; Rossello-Mora, R. *Int. J. Syst. Bacteriol.* **1998**, *48*, 179−186.
(6) Weiner, R. M.; Segall, A. M.; Colwell, R. R. *Appl. Environ. Microbiol.* **1985**, *49*, 83−90.
(7) Roh, Y.; Zhang, C. L.; Vali, H.; Lauf, R. J.; Zhou, J.; Phelps, T. J. *Clays Clay Miner.* **2003**, *51*, 83−95.
(8) DiChristina, T.; Bates D.; Burns J.; Dale J.; Payne A. In *Biogeochemistry of Anoxic Marine Basins*; Neretin, L., Ed.; Kluwer Publishing Co.: Dordrecht, The Netherlands, 2006.
(9) DiChristina, T. J.; Fredrickson, J. K.; Zachara, J. M. *Rev. Mineral. Geochem.* **2005**, *59*, 27−52.
(10) Shashkov, A. S.; Torgov, V. I.; Nazarenko, E. L.; Zubkov, V. A.; Gorshkova, N. M.; Gorshkova, R. P.; Widman, G. *Carbohydr. Res.* **2002**, *337*, 1119−1127.
(11) Kilcoyne, M.; Shashkov, A. S.; Perepelof, A. V.; Nazarenko, E. L.; Gorshkova, R. P.; Ivanova, E. P.; Widman, G.; Savage, A. V. *Carbohydr. Res.* **2005**, *340*, 1557−1561.
(12) Silipo, A.; Leone, S.; Molinaro, A.; Struiale, L.; Garozzo, D.; Nazarenko, E. L.; Gorshkova, R. P.; Ivanova, E. P.; Lanzetta, R.; Parrilli, M. *Eur. J. Org. Chem.* **2005**, 2281−2291.
(13) Korenevsky, A. A.; Vinogradov, E.; Gorby, Y.; Beveridge, T. J. *Appl. Environ. Microbiol.* **2002**, *68*, 4653−4657.
(14) Shashkov, A. S.; Senchenkova, S. N.; Nazarenko, E. L.; Zubkov, V. A.; Gorshkova, N. M.; Knirel, Y. A.; Gorshkova, R. P. *Carbohydr. Res.* **1997**, *303*, 333−338.
(15) Vinogradov, E.; Nossova, L.; Korenevsky, A.; Beveridge, T. J. *Carbohydr. Res.* **2005**, *340*, 1750−1753.
(16) Kostka, J. E.; Nealson, K. H. In *Techniques in Microbial Ecology*; Burlage, R. S., Atlas, R., Stahl, D., Geesey, G. G., Sayler, G., Eds.; Oxford University Press: Oxford, 1999; pp 58−78.
(17) Ohshima, H. *J. Colloid Interface Sci.* **2000**, *228*, 190−193.
(18) Duval, J. F. L.; Busscher, H. J.; van de Belt-Gritter, B.; van der Mei, H. C.; Norde, W. *Langmuir* **2005**, *21*, 11268−11282.
(19) Bos, R.; van der Mei, H. C.; Busscher, H. J. *Biophys. Chem.* **1998**, *74*, 251−255.

(20) Jiang, W.; Saxena, A.; Song, B.; Ward, B. B.; Beveridge, T. J.; Myneni, S. C. B. *Langmuir* **2004**, *20*, 11433−11442.
(21) Parker F.S. In *Applications of infrared, Raman, and resonance Raman spectroscopy in biochemistry*; Plenum Press: New York, 1983.
(22) Rouxhet, P. G.; Genet, M. J. In *Microbial Cell Surface Analysis, Structural and Physiochemical Methods*; Mozes, N., Handley, P. S., Busscher, H. J., Rouxhet, P. G., Eds.; VCH Publishers Inc.: New York, 1991; pp 173−220.
(23) Dague, E.; Duval, J.; Jorand, F.; Thomas, F.; Gaboriaud, F. *Biophys. J.* **2006**, *90*, 2612−2621.
(24) Beech, I.; Hanjagsit, L.; Kalaji, M.; Neal, A. L.; Zinkevich, V. *Microbiology* **1999**, *145*, 1491−1497.
(25) Nealson, K. H.; Myers, C. R. *Appl. Environ. Microbiol.* **1992**, *58*, 439−443.
(26) Neal, A. L.; Bank, T. L.; Hochella, M. F.; Rosso, K. M. *Geochem. Trans.* **2005**, *6*, 77−84.
(27) Schembri, M. A.; Dalsgaard, D.; Klemm, P. *J. Bacteriol.* **2004**, *186*, 1249−1257.
(28) de Windt, W.; Gao, H.; Krömer, W.; van Damme, P.; Dick, J.; Mast, J.; Boon, N.; Zhou, J.; Verstraete, W. *Microbiology* **2006**, *152*, 721−729.
(29) Bitton, G.; Friehofer, V. *Microbiol. Ecol.* **1978**, *4*, 119−125.
(30) Mittelmann, M. W.; Geesey, G. G. *Appl. Environ. Microbiol.* **1985**, *49*, 846−851.
(31) Geesey, G. G.; Bremer, P. J.; Smith, J. J.; Meugge, M.; Jang, L. K. *Can. J. Microbiol.* **1992**, *38*, 785−793.
(32) Labare, M. L.; Coon, S. L.; Matthais, C.; Weiner, R. M. *Appl. Environ. Microbiol.* **1997**, *63*, 4107−4110.
(33) Volesky, B.; Holan, Z. R. *Biotechnol. Prog.* **1995**, *11*, 235−250.

BM060826E